LIQUID CRYSTALS, 2016
VOL. 43, NO. 1, 112–123
http://dx.doi.org/10.1080/02678292.2015.1066888

Taylor & Francis
Taylor & Francis Group

Thermal characterisation of thermotropic nematic liquid-crystalline elastomers

David Thomas[a], Matt Cardarelli[a], Antoni Sánchez-Ferrer[b], Badel L. Mbanga[a], Timothy J. Atherton[a] and Peggy Cebe[a]

[a]Department of Physics and Astronomy, Center for Nanoscopic Physics, Tufts University, Medford, MA 02155, USA; [b]Department of Health Sciences and Technology, ETH, Zürich, Switzerland

ABSTRACT

Nematic liquid-crystalline elastomers (LCEs) are weakly cross-linked polymeric networks that exhibit rubber elasticity and liquid-crystalline orientational order due to the presence of mesogenic groups. Three end-on side-chain nematic LCEs were investigated using real-time synchrotron wide-angle X-ray scattering (WAXS), differential scanning calorimetry (DSC), and thermogravimetry (TG) to correlate the thermal behaviour with structural and chemical differences among them. The elastomers differed in cross-linking density and mesogen composition. Thermally reversible glass transition temperature, T_g, and nematic-to-isotropic transition temperature, T_{ni}, were observed upon heating and cooling. By varying the heating rate, T_g^0 and T_{ni}^0 were determined at zero heating rate. The temperature dependence of the orientational order parameter was determined from the anisotropic azimuthal angular distribution of equatorial reflections seen during real-time WAXS. Results show that the choice of cross-linking unit, its shape, density, and structure of co-monomers, all influence the temperature range over which the thermal transitions take place. Including multi-ring aromatic groups as cross-linkers increased the effective stiffness of the cross-linking, resulting in a higher glass transition temperature. The nematic-to-isotropic transition temperature increased in the presence of multi-ring aromatic structures, as either cross-linkers or mesogens, particularly when the multi-ring structures were larger than the low-molar-mass mesogen common to all three samples.

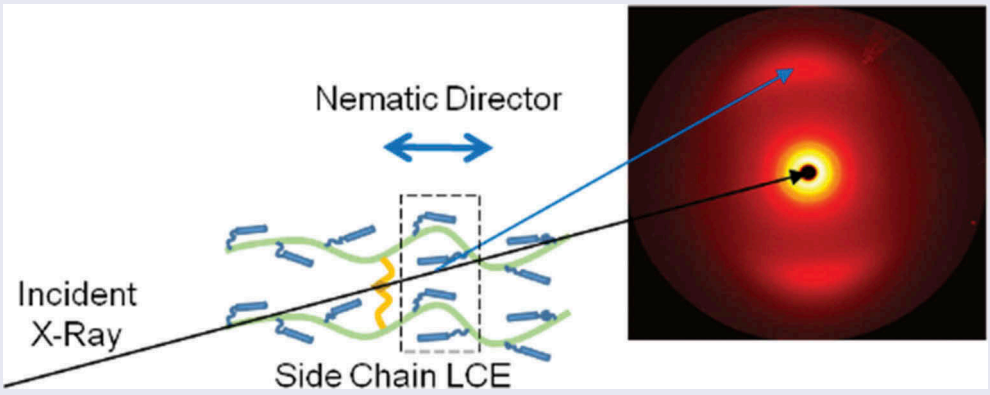

ARTICLE HISTORY
Received 15 April 2015
Accepted 24 June 2015

KEYWORDS
Side-chain liquid-crystalline elastomer; temperature-modulated differential scanning calorimetry; thermogravimetric analysis; wide-angle X-ray scattering; orientational order

Introduction

Liquid-crystalline elastomers (LCEs) are highly versatile materials with unique properties arising from the coupling of the rubber-like elasticity and the liquid-crystalline phase. As a result of this coupling, mechanical deformations result in changes to the local orientational order of the mesogens. The reverse transitions also occur: the response of the mesogens to stimuli such as heat, electric fields, or light can result in a mechanical response.[1–3] These materials are formed with mesogenic units embedded in a weakly cross-linked polymer network either as part of the polymer backbone (main chain) or as side groups branching off the polymer backbone (side chain).[2,3] This combined effect allows these materials to withstand very large strains and shear deformations.[3,4]

The particular samples discussed in this paper belong to the subset of LCEs known as thermotropic nematic side-chain liquid-crystalline elastomers (SCLCEs). SCLCEs contain mesogens as pendant side groups off the main polymer backbones, which form a

CONTACT Antoni Sánchez-Ferrer antoni.sanchez@hest.ethz.ch; Peggy Cebe peggy.cebe@tufts.edu

weakly cross-linked network.[1] When the density of cross-links is low, as is the case here, the mesogens will arrange into liquid-crystalline mesophases. Because the system is thermotropic, the mesogens undergo temperature-dependent phase transition from the nematic to isotropic phase at a temperature that depends not only on the particular mesogen but also on the cross-linking density.[5]

By selecting appropriate functional groups for the mesogens and the cross-linkers, it is possible to create different materials that mechanically respond to heat, light, magnetic, or electric fields. This has led to the creation of SCLCEs for applications including mechanically tunable optical systems, forming small actuators or generators, and creating new types of displays.[6–25] In recent years many SCLCEs have been synthesised with azobenzene structures as cross-linkers and/or mesogens, which has led to materials with coupled opto-mechanical properties.[6–13,22–25] These azobenzene compounds respond to light by undergoing a reversible *trans*→*cis* photo-isomerisation, where they become bent in shape, thereby lowering the nematic order and changing the mechanical response of the material.[7] In their relaxed *trans*-state, the azobenzene molecules act as rigid rod-like molecules that contribute to the overall nematic order in the same manner as any other mesogen. Azobenzene-dyed materials have been shown to act as optically controlled actuators,[6–25] which have been used to make micropumps and valves,[20] and show great potential in creating artificial muscles,[13–16] and are candidates for creating haptic displays.[9,17]

The thermal properties of various azobenzene-dyed thermotropic SCLCEs have been studied by wide-angle X-ray scattering (WAXS), differential scanning calorimetry (DSC), and polarising optical microscopy (POM).[8,11,17–20,25] In this paper we investigated a series of three SCLCEs with azobenzene groups present in various concentrations, as both mesogens and cross-linkers, which had been synthesised to investigate their opto-mechanical responses.[9–11,22,23,25] The nematic-to-isotropic transition is partially first order in these systems and the specific temperature and temperature range over which the transition occurs depend upon the chemical composition of the elastomer, the concentration and chemical structures of the cross-linkers, and the mesogens present. The response observed in DSC is known to be broader and more diffuse for elastomeric systems. This arises due to the quenching of sites of random disorder induced by the cross-links, which serve to broaden the thermal transitions.[19,20]

In addition to a basic mesogen and cross-linker, the three SCLCEs discussed in this paper contained varied azobenzene cross-linkers and azobenzene mesogens. For two of the three samples, the total concentration of cross-links and mesogenic units was fixed; in the third sample, the overall cross-linking density was reduced. We used real-time synchrotron X-ray scattering experiments during heating, and temperature-modulated DSC, to characterise how these structural variations led to the differences in both thermal properties and mesogenic ordering.

Experimental section

Materials

The three samples selected for this study are nematic end-on side-chain LCEs, called SCE03, SCE14, and SCE17, which were synthesised at the Institute for Macromolecular Chemistry, Albert Ludwigs University, Freiburg, Germany. Details of the synthesis are available in the literature.[9–12] Figure 1 shows the chemical structures of these materials. Samples were

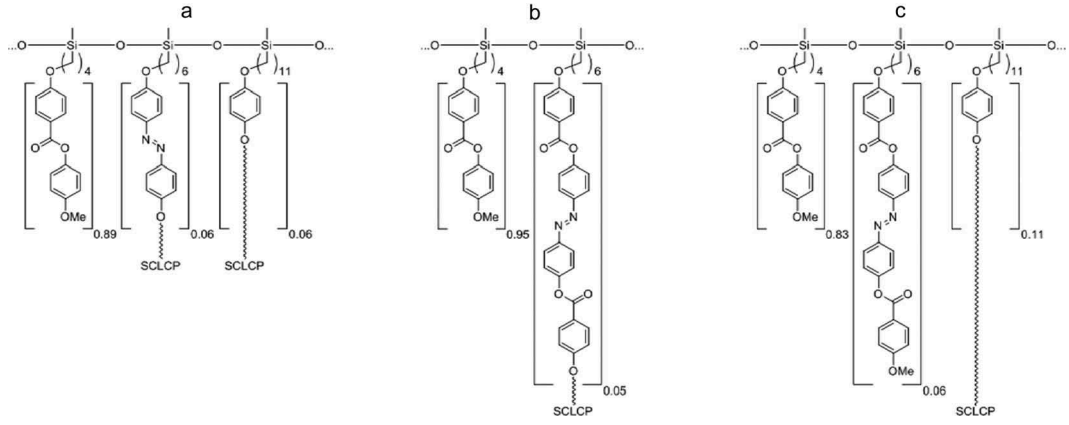

Figure 1. Chemical composition for SCLCE samples: (a) SCE03, (b) SCE14, and (c) SCE17. Values in brackets next to each pendant group refer to the concentration in mol-% © [2011 WILEY-VCH Verlag GmbH & Co. KGaA, 69469 Weinheim]. Reproduced by permission of John Wiley and Sons from [11].

prepared with varying mesogenic pendant groups and cross-linkers. The materials comprise the mesogen, 4-methoxyphenyl 4-(but-3-en-1-yloxy)benzoate (M4O Me,[17,19] MPBB) [11]; the isotropic cross-linker, 1,4-bis(undec-10-en-1-yloxy)benzene (SCC) [11]; and the flexible polymer backbone, poly(methylhydrogensiloxane) (PMHS).[11] The samples also include azobenzene molecules, which are the cross-linkers in SCE03 and SCE14, and the co-monomer in SCE17. The SCE03 elastomer contained 5.6 mol-% of two-aromatic ring azobenzene cross-linker, Azo2-c [11]; 5.6 mol-% of the isotropic cross-linker SCC; and 88.9 mol-% of MPBB, exclusive of the polymer backbone. The second sample, SCE14, contained 5.3 mol-% of four-aromatic ring azobenzene cross-linker, Azo4-c [11]; no isotropic cross-linker SCC; and 94.7 mol-% of MPBB. The third sample, SCE17, contained 11.1 mol-% isotropic cross-linker SCC; 5.6 mol-% of four-aromatic rings azobenzene mesogen Azo4-p [11]; and 83.3 mol-% of MPBB, exclusive of the polymer backbone. Both SCE03 and SCE17 had the same total mol-% of cross-linker and the same total mol-% of mesogenic units; however, the specific chemistry of these two components varied.[9–11]

Thermal analysis

To determine the thermal stability of the LCEs, thermogravimetry (TG) experiments were performed on a TA Instruments Q500 series thermogravimetric analyser from 30°C to 800°C at a heating rate of 20°C min^{-1}, under nitrogen gas flow at a rate of 50 mL min^{-1}.

Both DSC and its temperature-modulated variant (TMDSC) were performed on a TA Instruments Q100 series DSC equipped with a TA Instruments Refrigerated Cooling System. Small amounts (approximately 2–5 mg) of each sample were sealed in standard aluminium DSC pans. The pans were first rinsed in methanol to remove any oils that could have been deposited due to manufacturing and handling. Standard DSC runs were performed on each sample: six heating and cooling cycles were performed at different rates over the temperature range from −50°C to 130°C, with the exception of SCE14, which spanned the range from −50°C to 150°C. All three samples were brought through the temperature range at 2, 5, 10, 15, 20, and 25°C min^{-1}. The sample masses for the standard DSC experiments were about 5 mg. One TMDSC cycle was performed for each sample with lighter masses of approximately 2 mg at a heating and cooling rate of 5°C min^{-1} with a temperature-modulation amplitude of ±0.796°C and a period of 60 s. The DSC cell was purged with nitrogen at a flow rate of 50 mL min^{-1}. The cell was calibrated for temperature and heat flow accuracy using indium standard, and for heat capacity using sapphire standard. Analysis of the TG and DSC data was performed using TA Instruments Universal Analysis 2000 and MATLAB™ (from Mathworks).

Synchrotron WAXS

Real-time synchrotron WAXS experiments were performed on beam line X27C at the Brookhaven National Laboratory's National Synchrotron Light Source NSLS-I. A Mettler Toledo FP82HT hot stage paired with a Mettler Toledo FP90 Central Processor was used to control the heating and cooling of the samples. The LCE samples were mounted in the hot stage under one layer of Kapton™ high-temperature tape and aligned such that the nematic director was approximately horizontal. Aligned samples were heated to 130°C and held isothermally for 15 min, then cooled at a rate of 3°C min^{-1} to 50°C. The samples equilibrated at 50°C for approximately 2 min, and subsequently were heated from 50°C to 130°C at the rate of 3°C min^{-1}, held at 130°C for approximately 2 min, and then cooled to 50°C at the rate of 3°C min^{-1}. Finally, the samples were heated once again to 130°C at the rate of 3°C min^{-1}. Real-time data were collected at approximately two frames per minute with 23.5 s of exposure time per frame. Temperature and upstream (incident) intensity were recorded periodically on a MAR CCD 165 detector, while frames were collected continuously for each heating and cooling event. The isothermal hold and first controlled cooling and reheating were performed to rejuvenate the samples and remove any biases from the handling of the samples while being mounted in the hot stage.

The X-ray wavelength was λ = 0.1371 nm and the sample-to-detector distance was 15.94 cm. The scattering vector, q (where $q = 4\pi\sin\theta/\lambda$, for θ the half-scattering angle), was calibrated using Al_2O_3 standard reference powder. Intensity was corrected for Kapton™ background.

Results and discussion

Thermal analysis

TG was performed to determine the upper limit stability temperature of SCE03, SCE14, and SCE17. As shown in Figure 2a, both samples were thermally stable up to moderately high temperatures, around 175°C. SCE03 proved to be slightly more tolerant of high temperatures, retaining at least 97% of its weight until 400°C. Between 185°C and 225°C a small amount of

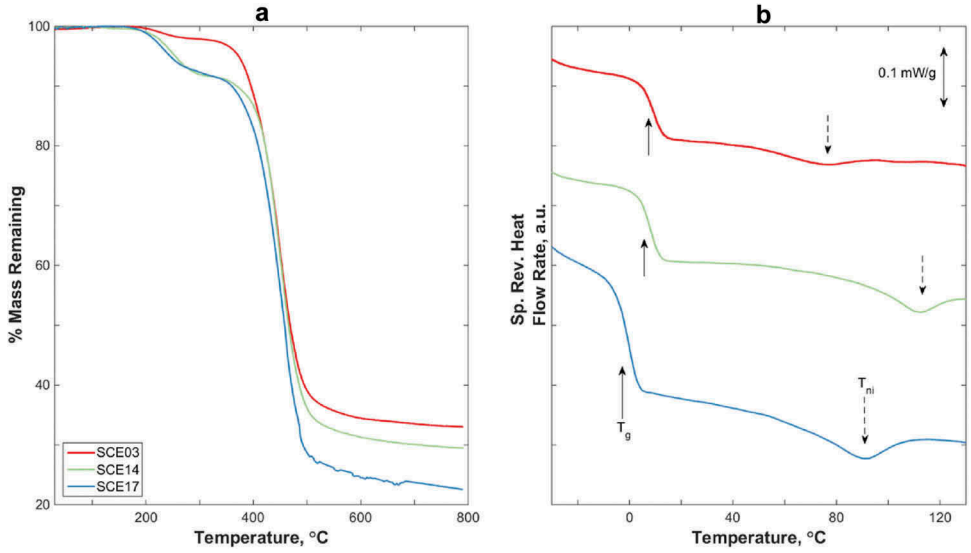

Figure 2. (colour online) Thermal data for SCE03 (red), SCE14 (green), and SCE17 (blue) during heating. (a) TG curve showing mass remaining vs. temperature at a heating rate of 20°C min^{-1}. (b) Specific reversing heat flow rate at a heating rate of 5°C min^{-1}. Arrows mark the approximate locations of T_g (solid arrow) and T_{ni} (dashed arrow). The curves have been displaced vertically for clarity.

mass is lost (about 2%). SCE14 and SCE17 showed a similar initial drop in mass above 188 and 175°C, respectively, and then remained stable before rapidly losing mass at temperatures in excess of 400°C. The degradation temperatures, T_{d1} and T_{d2}, are listed in Table 1 and correspond to the point where the % mass remaining first begins to decrease. The upper-limit temperatures for DSC studies on SCE03, SCE14, and SCE17 were set at 130°C, 150°C, and 130°C, respectively.

We performed TMDSC experiments to determine the glass transition temperature, T_g; the heat capacity increment, ΔC_p, evaluated at the glass transition; and T_{ni}, the nematic-to-isotropic transition temperature (often referred to as the clearing temperature, T_c). Results are shown in Figure 2b and Table 1.

To allow scanning at rates faster than those available with temperature-modulated DSC, a series of standard (non-modulated) DSC scans were performed between −50°C and 130°C (−50°C and 150°C for SCE14) at heating rates from 2 to 25°C min^{-1} (Figure 3).

Transition temperatures, T_g and T_{ni}, are shown as functions of heating rate in Figure 4a and 4b, respectively. T_g was determined from the inflection point and T_{ni} from the local minima, which for a first-order phase transition appears as a small endothermic peak at higher temperature than T_g. At the slowest heating rate, T_{ni} was not distinguishable from the noise level. T_{ni} was determined from the endpoint temperature, i.e., from the first departure point of the endothermic peak from the heat flow baseline following the nematic-to-isotropic transition. The latent heat was determined by integration of the endotherm.

Extrapolation of the data in Figure 4 (shown by the dashed lines) allows us to determine T_g^0 and T_{ni}^0, the values of these parameters at zero heating rate. We found T_g^0 = 8.6°C (SCE03), T_g^0 = 7.7°C (SCE14), and T_g^0 = −0.3°C (SCE17). The values of the nematic-to-

Table 1. Thermal properties of SCLCEs: degradation temperatures T_d, glass transition T_g, heat capacity increment ΔC_p, nematic-to-isotropic transition temperature T_{ni}, and latent heat $L°$.

	T_{d1} (°C)[a] ± 1°C	T_{d2} (°C)[a] ± 1°C	T_g^0 (°C)[b] ± 0.7 °C	ΔC_p (J g^{-1}°C^{-1})[c] ± 0.06 (J g^{-1}°C^{-1})	T_{ni}^0 (°C)[d]	L^0 (J g^{-1})[e] ± 0.1 (J g^{-1})
SCE03	185	310	8.6	0.35	85 ± 1	1.3
SCE14	188	320	7.7	0.41	121 ± 2	1.4
SCE17	175	360	−0.3	0.46	103 ± 1	1.9

[a]Determined from the peak of the derivative of the TGA curve at 20°C min^{-1}.
[b]Determined from the inflection point of the DSC curve extrapolated to a heating rate of 0°C min^{-1}.
[c]Determined from the difference between the extrapolated tangents to the glass and liquid-crystalline states, evaluated at T_g from the reversing heat flow curve at 5°C min^{-1}.
[d]Determined from the last departure point of the endothermic peak in the DSC curve from the liquid state baseline, extrapolated to a heating rate of 0° C min^{-1}.
[e]Determined from the area of the endothermic peak in the DSC curve extrapolated to a heating rate of 0°C min^{-1}.

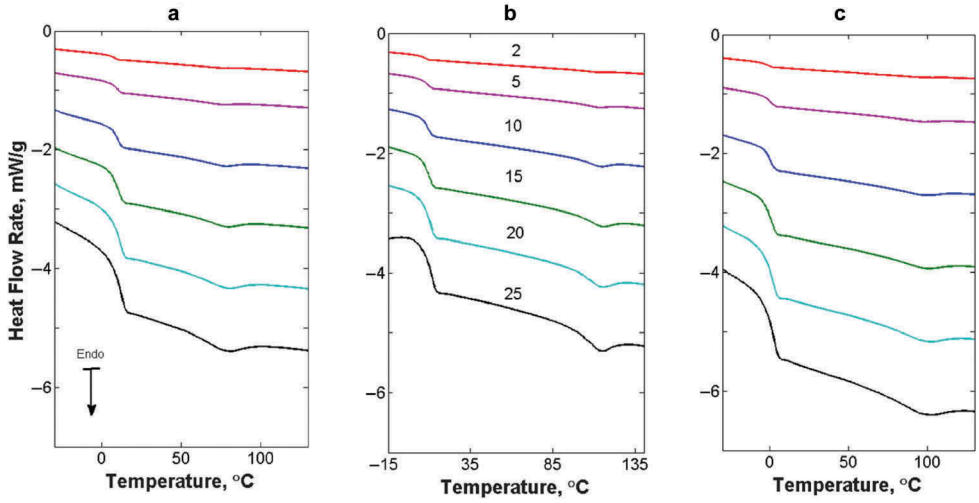

Figure 3. (colour online) DSC curves at various heating rates for: (a) SCE03, (b) SCE14, and (c) SCE17. From top to bottom the heating rates are: 2°C min^{-1} (red), 5°C min^{-1} (purple), 10°C min^{-1} (blue), 15°C min^{-1} (green), 20°C min^{-1} (cyan), and 25°C min^{-1} (black).

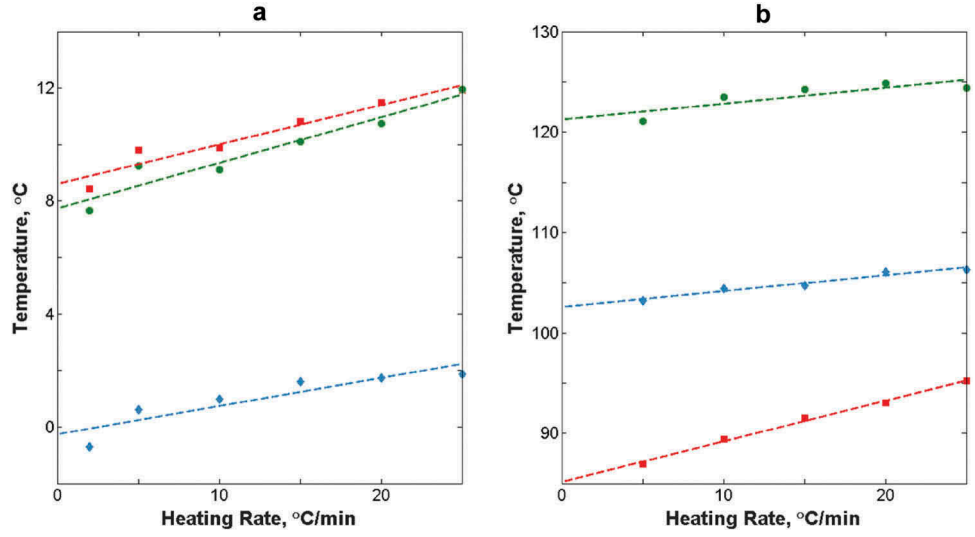

Figure 4. (colour online) Thermal properties vs. heating rate for SCE03 (red squares), SCE14 (green circles), and SCE17 (blue diamonds). (a) Glass transition temperature, T_g; (b) nematic-to-isotropic transition temperature, T_{ni}. Dashed lines represent best linear fits to the data.

isotropic transition were determined to be T_{ni}^0 = 85°C (SCE03), T_{ni}^0 = 121°C (SCE14), and T_{ni}^0 = 103°C (SCE17).

The glass transition temperature measured for SCE03 and SCE17 differs from the value of −2.0°C reported in the literature. The nematic-to-isotropic transitions were reported to occur at 85°C and 97°C for SCE03 and SCE17, respectively.[11] SCE14 was reported to have a glass transition temperature of 6.0°C and a nematic-to-isotropic transition of 113°C.[12] Following long storage periods all samples showed signs of ageing that only disappeared after heating and annealing above the nematic-to-isotropic transition temperature. The differences between the previously reported values for both the glass and nematic-to-isotropic transitions can be attributed to both differences in thermal analysis methods, as well as to the differences in chemical structure differences (e.g., possible transesterification above 120°C) at the time of measurement.

There were two main differences between these SCLCEs: the type of cross-linker and the type of mesogen. SCE14 and SCE17 each only had one type of cross-linker, the rigid azo4-c and the isotropic and flexible cross-linker SCC, respectively, as described in the literature.[9–12] SCE03 possessed not only the

isotropic cross-linker SCC but also a less-rigid azo2-c cross-linker.[9–12] The azobenzene cross-linkers can be regarded as molecularly 'stiffer' than the isotropic cross-linker SCC. The azo2-c cross-linker is a smaller and less-rigid molecule than the big and rigid azo4-c. Regarding the mesogen type, SCE03 and SCE14 only possessed one mesogen, MPBB, whereas SCE17 has a blend of both MPBB and the azo4-p mesogen as described in the literature.[9–12] These differences in molecular composition are reflected in the thermograms and transition temperatures.

A divergence of our polymeric materials from the expected behaviour of a low-molar-mass thermotropic liquid crystal can be seen in Figure 2. In low-molar-mass thermotropic liquid crystals, the phase change from an ordered, i.e., nematic, to a disordered isotropic state happens over a few degrees with a distinct endothermic peak at the transition temperature.[26–28] Embedding the mesogens in a weakly cross-linked polymer network significantly broadens the transition, due in part to polydispersity and chain conformation, causing the endothermic peaks to span a temperature interval of about 10 degrees at low rates and up to 40 at higher rates in the polymeric systems.

Synchrotron WAXS

X-ray scattering provides complementary insight as to how the mesogen and cross-linker composition of these elastomers give rise to the specific thermal properties observed in DSC. The real-time WAXS data allow for the characterisation of the molecular ordering present in the material as a function of temperature. The observed scattering pattern of all LCEs appears as two distinct meridional lobes (a typical intensity pattern is shown in Figure 5a for SCE17) when the elastomer is in the nematic phase.

The intensity in these lobes spreads into diffuse arcs as the elastomer begins its transition into the isotropic phase (Figure 5b). Following the phase change, as the amount of orientational order is reduced (Figure 5c), the intensity distribution appears as a ring, which is typical for an isotropic sample. We note that the azimuthal intensity distribution, measured at a fixed radius from the centre of reciprocal space, is always largest on the meridian. Taking intensity Figure 6 presents normalised WAXS intensity distributions obtained along the radial direction through the centres of the meridional lobes for the three samples. While

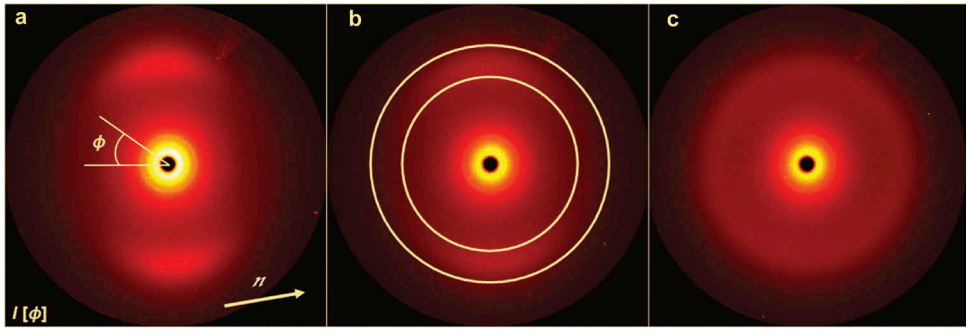

Figure 5. 2D WAXS intensity profile of SCE17 at different temperatures: (a) 53.6°C in the nematic phase; (b) 84.3°C at the inflection point of the nematic-to-isotropic transition; (c) 129.6°C in the isotropic phase. The yellow arrow in (a) indicates the nematic director. The yellow circles in (b) define the annulus used in radial integration of the azimuthal intensity distribution. (The irregular intensity seen in the upper right quadrant at about the one-o'clock position arises from a flaw in the detector.)

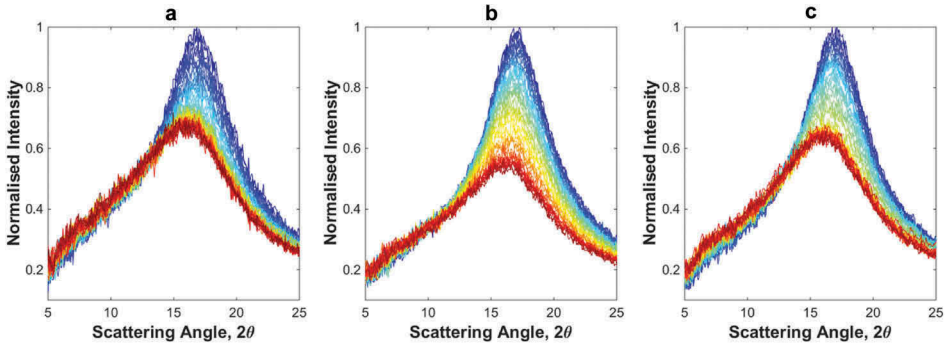

Figure 6. Normalised 1D WAXS radial intensity distributions for: (a) SCE03, (b) SCE14, and (c) SCE17. Colour scale indicates the relative temperature of the samples, with the blue curves representing the low-temperature limit at 50°C and the red curves representing the high-temperature limit at 130°C.

intensity is observed over a greater range of azimuthal angles as the samples are heated, the locations of the intensity maxima remain between 2θ = 15°–18°.

Common to all three samples is the decrease in overall intensity and shift of the 2θ peak position as the samples are heated. This is indicative of thermal expansion effects, polymer backbone chain conformational changes, and disordering of the mesogens upon heating. Both the mesogen-to-mesogen spacing and the backbone spacing were obtained from the scattering angle profiles for each sample in the nematic phase at 50°C, at the inflection point in the nematic-to-isotropic transition curves shown in Figure 9, and in the isotropic phase at 130°C (Table 2). As the samples are heated, the polymer backbone conformation changes towards a more random coil chain conformation as depicted in Figure 7. The conformational change of the backbone results in a disordering of the mesogens, which drives the system from the nematic to the isotropic phase.

Figure 5 shows the WAXS scattering patterns of SCE17 as it is brought from the nematic to the isotropic phase. The nematic scattering pattern (Figure 5a) results from mesogens being well ordered parallel to the polymer backbone as shown in Figure 7a. As the mesogens become disordered by heating, the X-rays are no longer scattered into two distinct meridional lobes; rather, they are scattered along diffuse arcs (Figure 5b) until the material is in the isotropic state (Figure 5c) in which the mesogens have random alignment and no longer remain predominantly parallel to the polymer backbone in the conformation shown in Figure 7b.

Table 2. WAXS d-spacing (±0.01 nm) for polymer backbone (d_{pb}) and mesogens (d_m) at different temperatures.

	T (°C)[a]	d_m (nm)	d_{pb} (nm)	T (°C)[b]	d_m (nm)	d_{pb} (nm)	T (°C)[c]	d_m (nm)	d_{pb} (nm)
SCE03	50	0.44	0.8	72.0	0.45	0.8	130	0.45	0.8
SCE14	50	0.44	0.8	109.5	0.45	0.8	130	0.45	0.8
SCE17	50	0.44	0.8	91.6	0.45	0.8	130	0.46	0.8

[a]Nematic state.
[b]At the inflection point of nematic-to-isotropic transition.
[c]Isotropic state.

The scattering patterns in Figure 5 are dependent upon the average orientations of the mesogens (and the mesogen-like cross-linkers that contribute to the molecular ordering). As the temperature increases, the mesogens become disordered, causing X-rays to be scattered through a greater range of azimuthal angles. The radii at which scattered intensity is observed were fixed for each sample to lie between 11° and 22.5° in 2θ. Radial integration over a circular annulus (Figure 5b) was performed using MATLAB^{TM}, to generate the intensity profile as a function of azimuthal angle, Figure 8. In order to quantify the degree to which these samples are ordered as a function of temperature, it is necessary to convert the intensity profile to a description of the molecular orientations of the mesogens.[29–35] Mitchell and Lovell,[29,30] and Leadbetter and Norris [31] have considered the problem of describing the mesogen orientation. They demonstrated a relationship between the intensity profile and the orientational distribution function (ODF), $f[\beta]$. The ODF describes how the distribution of the alignment of mesogens with respect to the director $\boldsymbol{n}$ gives rise to the scattering patterns seen in Figure 5.

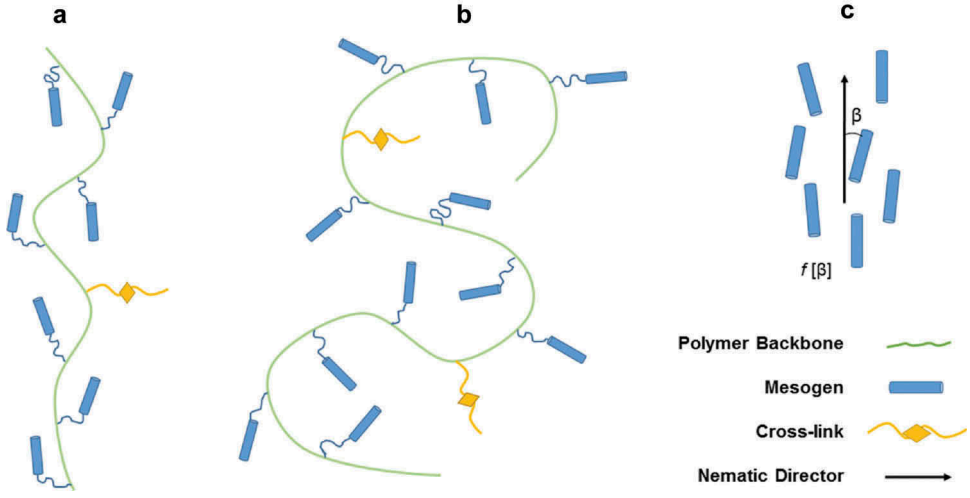

Figure 7. (colour online) Schematic of the polymer backbone and pendant mesogens. (a) At low temperatures in the nematic phase, the mesogens are aligned parallel to the polymer backbone. (b) At high temperatures in the isotropic phase, mesogens are randomly oriented and the polymer backbone adopts a more random coil conformation. (c) The distribution of mesogen orientations, represented by angle β, with respect to the nematic director, n, shown by an arrow.

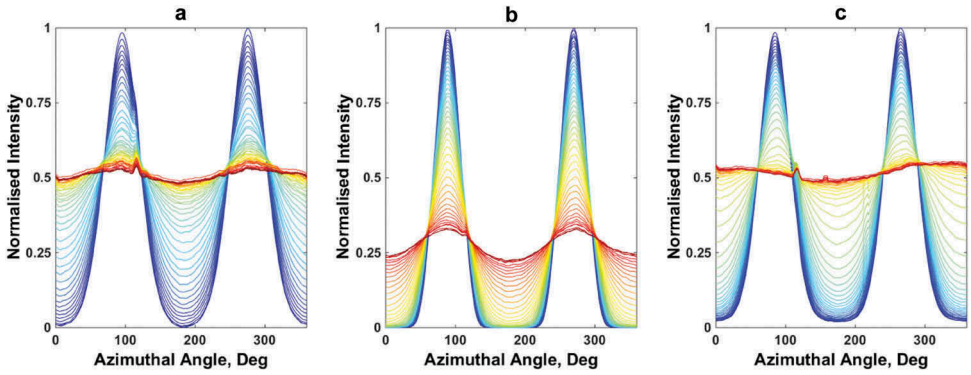

Figure 8. WAXS azimuthal intensity profiles during heating for: (a) SCE03, (b) SCE14, and (c) SCE17. Colour scale represents the temperature of the samples, with the blue curves representing the low temperature, nematic phase at 50°C, and the red curves representing high temperature up to 130°C. The tiny spike at around $\phi = 120°$ is an artefact from a defect on the CCD detector.

Based on the work carried out by Leadbetter and Norris,[31] Davidson *et al.* [33] demonstrated that the ODF can be expressed as a series of $\cos^{2n}(\phi)$ functions:

$$f[\beta] = \sum_{n=0}^{\infty} f_{2n} \cos^{2n}[\beta] \tag{1}$$

where n is an integer. The coefficients for the $\cos^{2n}(\phi)$ functions, f_{2n}, can be calculated directly by fitting the intensity profiles in Figure 6 to the following equation [33]:

$$I[\phi] = \sum_{n=0}^{\infty} f_{2n} \frac{2^2 n!}{(2n+1)!!} \cos^{2n}[\phi] \tag{2}$$

The ODF allows for direct calculation of the scalar order parameter, S, as shown below in Equations (3) and (4). The scalar order parameter is given by the average of the ODF over the second Legendre polynomial.[29–35] This quantity can vary from −0.5 to 1 with a value of −0.5 corresponding to a perfectly ordered oblate crystalline phase (oblate or perpendicular order), a value of zero corresponding to randomly oriented mesogens in the isotropic phase, and a value of unity corresponding to a perfectly prolate crystalline phase (prolate or parallel order).

$$\langle \cos^2[\beta] \rangle = \frac{\int_0^{\frac{\pi}{2}} f[\beta] \cos^2[\beta] \sin[\beta] \mathrm{d}\beta}{\int_0^{\frac{\pi}{2}} f[\beta] \sin[\beta] \mathrm{d}\beta} \tag{3}$$

$$S = \frac{1}{2}\left(3\langle \cos^2[\beta] \rangle - 1\right) \tag{4}$$

The order parameters in the nematic phase were obtained by averaging over the values from two data sets at the lower bound temperature of 50°C. The order parameters at the lower bound temperature for SCE03, SCE14, and SCE17 were 0.47, 0.77, and 0.62, respectively. The variation of the order parameter with temperature is shown in Figure 9.

SCE14 has a high-order parameter in the nematic phase at room temperature. Such large values could be indicative of a smectic mesophase, as has been observed, for instance, in siloxane-based LCEs. [36–38] Evidence for smectic mesophases in the siloxane elastomers was obtained using small-angle X-ray scattering (SAXS) and typical smectic layer spacings were reported to be between 4.5 and 4.9 nm.[36–38] Thus, in addition to our WAXS experiments, we also performed synchrotron SAXS studies on the three LCEs reported herein using a sample-to-detector distance of 1836.8 mm. We observed no scattering in the small-angle intensity patterns in the q-vector range corresponding to d-spacings from 1.6 to 8.0 nm. In the WAXS scattering patterns for SCE14, we observed only the meridional lobes shown in Figure 5, which correspond to orientational order and mesogen–mesogen periodicity. The SAXS and WAXS results taken together confirm that our LCE samples are all in the nematic phase at room temperature.

Comparing the DSC data of Figure 2b and Figure 3, with the order parameter data of Figure 9, there is a broadening of the nematic-to-isotropic transition resulting from the mesogens embedded in the lightly cross-linked polymer network. For a low-molecular-weight nematic liquid crystal, the nematic-to-isotropic transition would be sharper.[1,37,39–41] Transition breadth reflects the local variation in bonding environment. If most of the mesogens are embedded in a similar local environment, the transition will be sharper. If the local bonding environment varies, as would likely be the case with mesogens embedded in the polymer network, then the transition will be broadened. The order parameter vs. temperature curves in Figure 9 also lack the characteristic discontinuity or

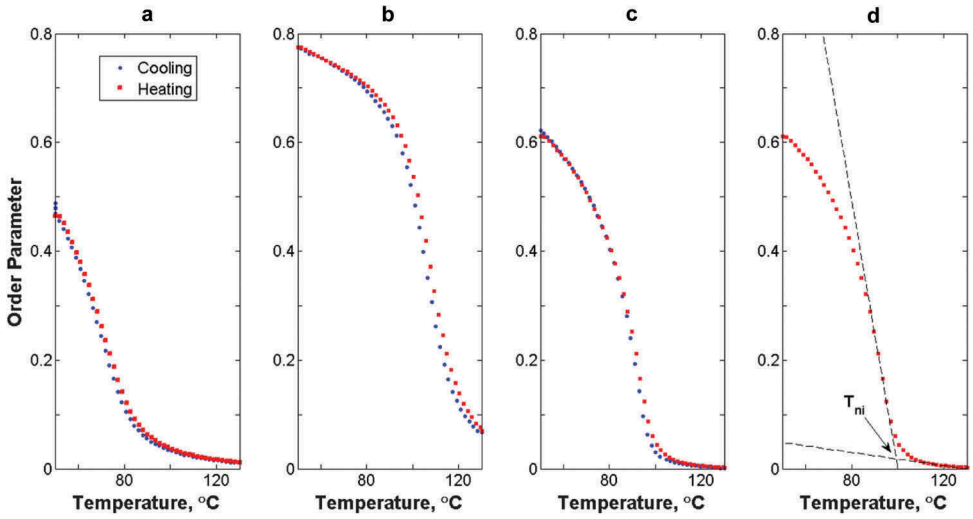

Figure 9. (colour online) Order parameter, *S*, as a function of temperature for SCLCEs upon cooling (blue) and heating (red) between 50°C and 130°C: (a) SCE03; (b) SCE14; (c) SCE17; and (d) SCE17 at 50°C and an example of the extrapolation method used to determine the nematic-to-isotropic transition temperature.

sharp change in slope as the sample enters the isotropic phase.[1,39–41] The lack of a sharp discontinuity at the nematic-to-isotropic transition as observed in conventional liquid crystals has received attention in recent work relying on nuclear magnetic resonance (NMR) measurements.[42–46] This work, on thermotropic liquid crystal elastomers, used NMR [42–46] to study residual orientational ordering that was present following departure from the nematic mesophase upon heating.[42–46] Orientational order parameters obtained from these NMR measurements show the same continuous behaviour as observed in WAXS measurements.

During the two-step cross-linking procedure,[4] these elastomers reported here are cross-linked in the nematic, aligned phase. As the mesogens are disordered and the backbone reorganises into a more random coil conformation, an internal stress field drives the nematic-to-isotropic transition into a supercritical regime, or a paranematic phase, where the values of the order parameter are small but non-zero.[42,43] As a result, the order parameter vs. temperature curve is continuous as the system transitions from the nematic phase to its final isotropic phase. The effect of this supercritical regime is minimal and the overall transition manifests as a first-order phase transition as there is a latent heat associated with the departure from the nematic phase.

In the order parameter vs. temperature plots, the nematic-to-isotropic transition was identified using the intersection between two tangents to the curve shown in Figure 9d. The first tangent line runs through the inflection point in the order parameter vs. temperature curve and the second tangent tracks the isotropic baseline following the supercritical range as the order parameter values decrease towards zero. These data points can be compared to the thermally determined transition temperatures identified at the endpoint of the endothermic peak by interpolating the data in Figure 4b to a heat rate of 3°C min^{-1}. The values obtained by this interpolation are in good agreement with those obtained at the intersection of tangents in the order parameter data. The transition temperatures determined by WAXS for cooling and heating and the interpolated values are recorded in Table 3.

SCE03 contained one mesogen, MPBB, and a mixture of two cross-linkers, the isotropic cross-linker SCC and a mesogenic cross-linker. The mesogenic cross-linker in this sample was a two-ring azobenzene molecule, azo2-c, similar in size to the MPBB mesogen. The addition of this azobenzene cross-linker created a polymer network 'stiffer' than a network with the same cross-linking concentration made of purely isotropic linkages. This resulted in the highest glass

Table 3. Nematic-to-isotropic transition temperature T_{ni} and average order parameter *S* in the nematic phase at 50°C.

	T_{ni} (°C) ± 1°C Cooling[a]	T_{ni} (°C) ± 1°C Heating[a]	S ± 0.1	T_{ni} (°C) ± 2°C Heating[b]
SCE03	85	86	0.5	86
SCE14	120	123	0.8	122
SCE17	98	99	0.6	103

[a]Determined from the order parameter vs. temperature curves for heating and cooling rates of 3°C min^{-1} obtained by WAXS experiment.
[b]Interpolated nematic-to-isotropic transition temperatures for a heating rate of 3°C min^{-1} obtained by DSC experiments.

transition temperature observed in the three samples. While the azobenzene cross-linker contributes to the nematic ordering of the mesogens, it does not have as high a nematic-to-isotropic transition, and does not bring the transition temperature to the range of SCE14 or SCE17 as the mesogens and azobenzene groups are of similar size. As seen in Figure 3b the nematic-to-isotropic transition endotherm begins just after 50°C and this can be seen in Figure 9a as the order parameter sharply decreases between 50°C and 70°C.

SCE17 has the same total mesogen and cross-linking concentration as SCE03. This sample only possesses the isotropic cross-linker SCC resulting in a less-'rigid' polymer network with the lowest glass transition temperature of the three samples. From Figure 9c, it can be seen that this sample is more ordered than SCE03 while exhibiting a behaviour similar to that of a low-molar-mass liquid crystal. This is due to the presence of the four-ring azobenzene mesogens azo4-p intermixed with the MPBB throughout the sample along with minimal constraint from the isotropic cross-linker. The larger mesogen stabilises the nematic phase requiring both a higher temperature to induce the phase transition to an isotropic liquid and more energy per unit mass than either of the other samples (see Table 1). Further evidence of the effect of larger mesogenic structures being added to the network can be seen in the change in heat capacity at the glass transition. The heat capacity increment is the largest for this sample as it has the greatest concentration of four aromatic rings of all three samples, which become free to rotate and move once out of the vitreous state.

SCE14 differed from the other two samples in that it had less than half the total cross-linking concentration. Despite having the lowest concentration of cross-linker, the four-ring azobenzene structure was the most 'rigid' cross-linker azo4-c present among the samples. Figure 4a illustrates this, as SCE14 has a glass transition temperature similar to SCE03. Similar to SCE17, the heat capacity increment at the glass transition is higher than that of SCE03 due to the presence of the four aromatic rings core. These 'rigid' cross-linkers serve to stabilise the nematic phase to high temperatures. This results in the most ordered nematic phase as seen in Figure 9b.

Conclusions

The SCLCEs studied here varied in three constituent parameters: mesogen type, cross-linker type, and component concentration. Chemical structure differences affected the temperature ranges over which each sample underwent the glass-to-rubber and nematic-to-isotropic transitions. In order to observe the glass transition process, the polymer molecular chain must undergo changes in conformation brought about by free rotation about chemical bonds in the molecular chain, either in the backbone or in the side groups. The glass transition of the SCLCE materials studied here showed dependence on the density and rigidity of the cross-linker molecules present. Both SCE03 and SCE17 had more than double the concentration of cross-linkers compared to SCE14. However, SCE14 exhibited a higher glass transition temperature than SCE17. This can be attributed to the four-aromatic-ring azobenzene structure, which comprised the cross-linker in SCE14, and which was substantially more rigid than the isotropic cross-linker in SCE17. SCE03 possessed both the isotropic cross-linker and a two-aromatic-ring azobenzene cross-linker, which resulted in the highest glass transition temperature.

The nematic-to-isotropic liquid crystal phase transition is a first-order phase transition, which requires a latent heat. T_{ni} showed dependence on both the mesogen and cross-linker selection. The cross-linkers present in SCE03 and SCE14 (two- and four-ring azobenzene structures, respectively) contributed to the liquid-crystalline order of the material in the nematic liquid state. However, the two-ring azobenzene present in SCE03 did not impact the ordering to the same degree as the four-ring azobenzene structures present in SCE14 and SCE17. The four-ring azobenzene structures are effectively twice the length of the mesogen, MPBB, present in all three SCLCEs. The addition of these larger molecules results in a higher nematic-to-isotropic transition. In the case of SCE14 the four-ring azobenzene is present as the cross-linker but behaves also as a mesogen insofar as it contributes to the nematic ordering of the system. It is observed that while SCE14 had the highest nematic-to-isotropic transition, due to the ordering contribution of the mesogenic cross-linker, the latent heat of this phase change was very close to that of SCE03. SCE17 possesses a mixture of two mesogens and required the greatest amount of energy per unit mass to undergo the nematic-to-isotropic phase change. These results suggest that the latent heat will vary with the mesogen concentration and type, while the transition temperature will be affected by the ordering contributions of mesogenic cross-linkers.

These novel SCLC elastomers synthesised with the addition of various azobenzene molecules acting as either mesogenic units or cross-linkers afford the system the ability to undergo conformational changes in response to polarised light.[9–12,25] Understanding how their bulk

thermal properties and structural transitions are affected by the selection of azobenzene groups, it becomes possible to create responsive materials that have favourable thermal characteristics for industrial applications.

Acknowledgement

The authors thank Dr Lixia Rong and Dr Maya K. Endoh (Koga) for assistance with X-ray experiments.

Disclosure statement

No potential conflict of interest was reported by the authors.

Funding

Support for this research was provided in part by the National Science Foundation, Polymers Program of the Division of Materials Research, under [grant number DMR-1206010], and through the MRI Program under [grant number DMR-0520655], which provided thermal analysis instrumentation. A portion of this research was conducted at the Brookhaven National Synchrotron Light Source, beam line X27C, supported by the Department of Energy.

References

[1] Warner M, Terentjev EM. Liquid crystal elastomers. Clarendon: Oxford; 2007.
[2] Davis F. Liquid-crystalline elastomers. J Mater Chem. 1993;3:551–562.
[3] Terentjev EM. Liquid-crystalline elastomers. J Phys; Condens Matter. 1999;11:R239–R257. doi:10.1088/0953-8984/11/24/201
[4] Küpfer J, Finkelmann H. Nematic liquid single crystal elastomers. Macromol Chem, Rapid Commun. 1991;12:717–726. doi:10.1002/marc.1991.030121211
[5] Dubois JC, Le Barny P, Mauzac M, et al. Behavior and properties of side chain thermotropic liquid crystal polymers. Acta Polym. 1997;48:47–87. doi:10.1002/actp.1997.010480301
[6] Finkelmann H, Nishikawa E, Pereira GG, et al. A new opto-mechanical effect in solids. Phys Rev Lett. 2001;87:015501. doi:10.1103/PhysRevLett.87.015501
[7] Yu Y, Nakano M, Ikeda T. Photomechanics: directed bending of a polymer film by light. Nature. 2003;425:145. doi:10.1038/425145a
[8] Domenici V, Ambrožič G, Čopič M, et al. Interplay between nematic ordering and thermomechanical response in a side-chain liquid single crystal elastomer containing pendant azomesogen units. Polymer. 2009;50:4837–4844. doi:10.1016/j.polymer.2009.08.021
[9] Sánchez-Ferrer A. Light-induced disorder in liquid-crystalline elastomers for actuation. Proc. SPIE. 2011;8107:810702-1–810702-8.
[10] Sánchez-Ferrer A, Fischl T, Stubenrauch M, et al. Photo-crosslinked side-chain liquid crystalline elastomers for microsystems. Macromol Chem Phys. 2009;210:1671–1677. doi:10.1002/macp.v210:20
[11] Sánchez-Ferrer A, Merekalov A, Finkelmann H. Opto-mechanical effect in photoactive nematic side-chain liquid-crystalline elastomers. Macromol Rapid Commun. 2011;32:671–678. doi:10.1002/marc.v32.8
[12] Sánchez-Ferrer A. Photoactive Liquid-Crystalline Elastomers [dissertation]. Barcelona (ES): University of Barcelona; Freiburg (DE): University of Freiburg; 2007.
[13] Camacho-Lopez M, Finkelmann H, Palffy-muhoray P, et al. Fast liquid-crystal elastomer swims into the dark. Nat Mater. 2004;3:307–310. doi:10.1038/nmat1118
[14] Thomsen DL, Keller P, Naciri J, et al. Liquid crystal elastomers with mechanical properties of a muscle. Macromol. 2001;34:5868–5875. doi:10.1021/ma001639q
[15] Madden J, Vandesteeg N, Anquetil PA, et al. Artificial muscle technology: physical principles and naval prospects. IEEE J Oceanic Eng. 2004;29:706–728. doi:10.1109/JOE.2004.833135
[16] Buguin A, Li M, Silberzan P, et al. Micro-actuators: when artificial muscles made of nematic liquid crystal elastomers meet soft lithography. J Am Chem Soc. 2006;128:1088–1089. doi:10.1021/ja0575070
[17] Torras N, Zinoviev K, Esteve J, et al. Liquid-crystalline elastomer micropillar array for haptic actuation. J Mater Chem C. 2013;1:5183–5190.
[18] Selinger JV, Ratna BR. Isotropic-nematic transition in liquid-crystalline elastomers: lattice model with quenched disorder. Phys Rev E. 2004;70:041707. doi:10.1103/PhysRevE.70.041707
[19] Garcia-Amorós J, Finkelmann H, Velasco D. Influence of the photo-active azo cross-linker spacer on the opto-mechanics of polysiloxane elastomer actuators. J Mater Chem. 2011;21:1094–1101. doi:10.1039/C0JM02502J
[20] Garcia-Amoros J, Velasco D. Understanding the fast thermal isomerization of azophenols in glass and liquid crystalline polymers. Phys Chem Chem Phys. 2014;16:39–52.
[21] Tajbakhsh AR, Terentjev EM. Spontaneous thermal expansion of nematic elastomers. Eur Phys J E. 2001;6:181–188.
[22] Sánchez-Ferrer A, Fischl T, Stubenrauch M, et al. Liquid-crystalline elastomer microvalve for microfluidics. Adv Mater. 2011;23:4526–4530. doi:10.1002/adma.201102277
[23] Li X, Fang L, Hou L, et al. Photoresponsive side-chain liquid crystalline polymers with amide group-substituted azobenzene mesogens: effects of hydrogen bonding, flexible spacers, and terminal tails. Soft Matter. 2012;8:5532–5542.
[24] Tašič B, Li W, Sánchez-Ferrer A, et al. Light-induced refractive index modulation in photoactive liquid-crystalline elastomers. Macromol Chem Phys. 2013;214:2744–2751. doi:10.1002/macp.201300493
[25] Sánchez-Ferrer A, Finkelmann H. Opto-mechanical effect in photoactive nematic main-chain liquid-crystalline elastomers. Soft Matter. 2013;9:4621–4627.
[26] Oweimreen GA, Morsy MA. DSC studies on p-(n-alkyl)-p′-cyanobiphenyl (RCB's) and p-(n-alkoxy)-p′-cyanobiphenyl (ROCB's) liquid crystals. Thermo Acta. 2000;346:37–47. doi:10.1016/S0040-6031(99)00411-6

[27] Neuenfeld S, Schick C. Verifying the symmetry of differential scanning calorimeters concerning heating and cooling using liquid crystal secondary temperature standards. Thermochim Acta. 2006;446:55–65. doi:10.1016/j.tca.2006.05.005
[28] Wunderlich B. Thermodynamic properties. In: Seidel A, editor. Properties and behavior of polymers. Hoboken (NJ): Wiley; 2011. p. 1186–1229.
[29] Lovell R, Mitchell GR. Molecular orientation distribution derived from an arbitrary reflection. Acta Crystallogr Sec A. 1981;37:135–137. doi:10.1107/S0567739481000247
[30] Mitchell GR, Lovell R. Application of cylindrical distribution functions to wide-angle x-ray scattering from oriented polymers. Acta Crystallogr Sec A. 1981;37:189–196. doi:10.1107/S0567739481000478
[31] Leadbetter AJ, Norris EK. Distribution functions in three liquid crystals from x-ray diffraction measurements. Mol Phys. 1979;38:669–686. doi:10.1080/00268977900101961
[32] Leadbetter AJ, Wrighton PG. Order parameters In S_a, S_c and n phases by X-ray diffraction. Jl De Physique. 1979;40:234–242.
[33] Davidson P, Petermann D, Levelut AM. The measurement of the nematic order parameter by x-ray scattering reconsidered. J Phys II France. 1995;5:113–131. doi:10.1051/jp2:1995117
[34] Giesselmann F, Germer R, Saipa A. Orientational order in smectic liquid-crystalline phases of amphiphilic diols. J Chem Phys. 2005;123:034906.
[35] Sanchez-Castillo A, Osipov MA, Giesselmann F. Orientational order parameters in liquid crystals: a comparative study of X-ray diffraction and polarized Raman spectroscopy results. Phys Rev E. 2010;81:021707. doi:10.1103/PhysRevE.81.021707
[36] Aksenov V, Bläsing J, Stannarius R, et al. Strain-induced compression of smectic layers in free-standing liquid crystalline elastomer films. Liq Cryst. 2005;32:805–813. doi:10.1080/02678290500161363
[37] Rössle M, Braun L, Schollmeyer D, et al. Differences between smectic homo- and co-polysiloxanes as a consequence of microphase separation. Liq Cryst. 2005;32:533–538. doi:10.1080/02678290500115724
[38] Ahn S, Deshmukh P, Gopinadhan M, et al. Side-chain liquid crystalline polymer networks: exploiting nanoscale smectic polymorphism to design shape-memory polymers. ACS Nano. 2011;5:3085–3095. doi:10.1021/nn200211c
[39] Sengupta A. Topological microfluidics: nematic liquid crystals and nematic colloids in microfluidic environment. Heidelberg: Springer; 2013.
[40] Kurochkin O, Atkuri H, Buchnev O, et al. Nanocolloids of Sn2P2S6 in nematic liquid crystal pentylcianobiphenile. Condensed Matter Phys. 2010;13:33701.
[41] Quan L. Liquid crystals beyond displays. Hoboken (NJ): John Wiley & Sons; 2012.
[42] Selinger JV, Jeon HG, Ratna BR. Isotropic-nematic transition in liquid-crystalline elastomers. Phys Rev Lett. 2002;89:225701. doi:10.1103/PhysRevLett.89.225701
[43] Lebar A, Kutnjak Z, Žumer S, et al. Evidence of supercritical behavior in liquid single crystal elastomers. Phys Rev Lett. 2005;94:197801. doi:10.1103/PhysRevLett.94.197801
[44] Domenici V. 2H NMR studies of liquid crystal elastomers: macroscopic vs. molecular properties. Prog Nucl Magn Reson Spectrosc. 2012;63:1–32. doi:10.1016/j.pnmrs.2011.07.003
[45] Cifelli M, Domenici V, Veracini CA. Recent advancements in understanding thermotropic liquid crystal structure and dynamics by means of NMR spectroscopy. Curr Opin Colloid Interface Sci. 2013;18:190–200. doi:10.1016/j.cocis.2013.03.003
[46] Domenici V, Milavec J, Zupančič B, et al. Brief overview on 2H NMR studies of polysiloxane-based side-chain nematic elastomers. Magn Reson Chem. 2014;52:649–655. doi:10.1002/mrc.v52.10